

Supplementary Material for
A base pair resolution map of nucleosome positions in yeast

Kristin Brogaard¹, Liqun Xi², Ji-Ping Wang^{2,*}, and Jonathan Widom^{1,3}

¹Department of Molecular Biosciences, Northwestern University, Evanston, IL, 60208, USA

²Department of Statistics, Northwestern University, Evanston, IL, 60208, USA

³Department of Chemistry, Northwestern University, Evanston, Illinois 60208, USA

*Correspondence should be addressed to J.P. Wang (jzwang@northwestern.edu)

Supplementary Methods

1. H4S47C *Saccharomyces cerevisiae* strain

The H4S47C *S. cerevisiae* strain was engineered in the BY4741 (*MATa, his3Δ1, leu2Δ0, met15Δ0, ura3Δ0*) background. The H4S47C mutation was made in the *HHF1* gene. The second histone H4 gene, *HHF2*, was knocked out and replaced with the *ura3* selection marker.

2. *In vivo* chemical mapping

The H4S47C *S. cerevisiae* strain was grown in YPD (10% yeast extract, 20% peptone and 20% dextrose) to a density of $\sim 1.5 \times 10^7$ cells/ml. For a 500mL culture, cells were collected and quickly washed with 1M sorbitol and immediately resuspended in 5mL of permeabilizing buffer (1M sorbitol, 5mM BME and 0.5mg of lyticase Sigma cat# L5263vc-200KU) and incubated at room temperature with rotation for 5 minutes. Permeabilized cells were washed 2x in 5ml of 1M sorbitol with 0.1% NP-40 and resuspended in 2mL of labeling buffer (1M sorbitol, 50mM NaCl, 10mM Tris-HCl pH 7.5, 5mM MgCl₂, 0.5mM spermidine, 0.15mM spermine, 0.1% NP-40). Immediate permeabilization is necessary to deplete cellular ATP and minimize salts, reducing the capabilities of a nucleosome to shift positions^{3, 4, 5, 6}. We chose not to formaldehyde cross-link because of the potential effects cross-linking could have on the spatial positioning of the cysteine and the label in relation to the DNA backbone. The thiol reactive label - N(1,10 phenanthroline- 5-yl) iodoacetamide (Biotium cat# 92015), was dissolved in DMSO to a concentration of 7mM and added to the cells for a final concentration of 1.4mM of label and 20% total volume of DMSO. This concentration of DMSO was chosen to facilitate entry of the thiol reactive label into the cells. Research from several publications indicates that DMSO at this concentration does not affect protein-protein and protein-DNA interactions^{7, 8}. Additionally, we are not concerned about DMSO induced DNA melting because of the low temperature used during the labeling process⁹. The light-sensitive labeling reaction was incubated at room temperature, with rotation for 2 hours, and then overnight at 4°C. This reaction was then washed 2x in 10mL of 1M sorbitol and 0.1% NP-40, then resuspended in 1.5mL mapping buffer (1M sorbitol, 2.5mM NaCl, 50mM Tris-HCl pH 7.5, 5mM MgCl₂, 0.5mM spermidine, 0.15mM spermine and 0.1% NP-40). Cupric chloride (CuCl₂) was added to a final concentration of 150μM and incubated for 5min. The cells were washed 2x in 10mL of mapping buffer and resuspended in 1.5mL mapping buffer. Beta-mercaptopropionic acid (MPA) was added to a final concentration of 6mM, and incubated for 5min, reducing the copper to cuprous chloride. The chemical mapping reaction was then initiated by the addition of hydrogen peroxide to a final concentration of 6mM. The reaction was mixed well and incubated for 20 minutes. The

mapping reaction was quenched by the addition of Neocuprine (Sigma), 2.8mM final. Once quenched the cells were spun down and resuspended in 1mL of 1mM Tris-HCl pH 7.5 and 0.1mM EDTA. To disrupt histone-DNA contacts, SDS and NaCl were added to a final concentration of 2% and 2M respectively and incubated for 1 hour. DNA was purified by phenol-chloroform extraction and subsequent ethanol precipitation. The sample was RNased (1mg/ml final) overnight at 42°C and run on a 2% agarose gel. The shortest DNA band, corresponding to the center-to-center distance of two nucleosome neighbors, was cut out of gel and the DNA was extracted.

Although the cited references all suggest that the DMSO at the given concentration and given experimental conditions would not affect DNA-protein interactions (and thus not the DNA-histone binding), and the comparisons between the individual chemical maps and between chemical map and MNase maps show good consistency in nucleosome positions, we acknowledge that future experiments are needed to elucidate how the chemical mapping might be affected by different DMSO concentrations.

In our protocol we chose not to cross-link the chromatin to avoid introducing possible extra variability due to the cross-link procedure itself. The long incubation time however could, in principle, allow existing chromatin remodelers to shift nucleosomes to a positioning state that best facilitates the current function of the genome¹⁰. Although we believe that the effect due to non-cross-linking will not change the global landscape of the nucleosome map (as shown in **Fig. 4a**) future studies are needed to assess its effect on the detail of local positioning.

3. Preparation of mapped DNA fragment for ABI SOLiD sequencing.

The ends of the chemically mapped DNA were blunted using first NEB's Klenow Polymerase large fragment (cat # M0210L) then processed further using Lucigen's DNATerminator End Repair Kit (cat # 40035-2). The sequence of events in the blunting and phosphorylation of the mapped DNA ends is crucial for the subsequent analysis of the mapped products. Initial treatment with Klenow Polymerase large fragment first removes 3' overhangs and fills in 5' overhangs to create blunted DNA fragments. The use of a single polymerase, such as Klenow, creates a more homogenous set of DNA ends relative to the hydroxyl radical cleavage sites. Lucigen's DNATerminator End Repair Kit was used primarily for its phosphorylation abilities. However any possible residual overhanging DNA ends would be blunted by this treatment (the

kit blunts all single stranded DNA overhangs. ABI SOLiD adapters were ligated to the blunted and phosphorylated DNA ends. Nick translation and PCR amplification were completed following ABI's SOLiD Fragment Preparation protocol. All samples were sequenced with ABI's SOLiD next generation sequencing system. Six independent mapping experiments were sequenced – four using single end sequencing and two using paired end sequencing.

4. Isolation, preparation and sequencing of higher molecular weight DNA

To investigate the asymmetry of cleavages on different DNA strands we isolated and sequenced higher molecular weight DNA. After a single mapping experiment we extracted mapped DNA ranging in size from 200-500bp. Due to the size limitations for the insert DNA for ABI SOLiD sequencing (<250bp) the higher molecular weight DNA had to be shortened while maintaining the ends (the cleavage sites). To do this we followed the protocol described by Boyle et al.¹³. In short, this protocol captures blunted and phosphorylated chemically mapped ends by blunt-end ligation of a biotinylated sequencing adapter with an Mme1 endonuclease restriction site at the 5' end. By pulling down the biotinylated adapters all mapped ends were captured and enriched. The Mme1 endonuclease cleaves 18-20bp (2bp overhang) base pairs downstream into the genomic DNA, leaving only the first 18 - 20bp downstream of the cleavage sites. Ligation of second sequencing adapter leaves a DNA fragment short enough for sequencing. DNA products were nick translated and amplified following ABI's SOLiD Fragment Preparation protocol. These mapping products were sequenced by ABI SOLiD single-end sequencing.

5. Data

The sequencing reads from the six experiments were first mapped to the yeast genome (UCSC -SAC2 version). For all single-end samples we used Software Mapreads-2.4.1 for alignment allowing for 3 mismatches. For the paired end samples, we used Software BioScope-1.2.1 for alignment allowing for 3 mismatches for the F3 end and 2 mismatches for the F5 end. Each single-end read maps the cleavage site on one strand, while the paired-end reads map cleavage sites on the opposite strands simultaneously. Only reads that mapped to the genome at one unique location were kept for analyses to avoid ambiguity. We produced a map of 105 million cleavages in total for each strand from the six experiments. For the follow-up data with higher molecular weight DNA fragment, 12 million cleavages were mapped for each strand. The

raw cleavage frequency patterns from the single-end and paired-end experiments are highly consistent genome-wide (results not shown), so are the independent nucleosome maps generated from separate experiments based on a Bayesian devolution algorithm discussed below (Figure 3a). We therefore combined the six data sets and created a final unique map of 67,543 nucleosomes and a redundant map of 351,264 nucleosomes. All the analyses presented in this paper (unless indicated) are based on these two maps.

6. Primary and secondary sites confirmation

To identify the positions of major cleavage sites within a nucleosome (analogous to the primary and secondary cleavage sites described in the earlier work of Flaus and Richmond^{11, 12}), we calculated the frequency of observed cleavages at every genomic location for Watson (+ strand) and Crick (- strand) strands separately. A local frequency peak was first defined as one that must be a local maximum within +/-73 bp on one strand. We then selected unique peaks sequentially for each strand in descending order of peak height requiring that no two peaks be positioned within 147 bp. The frequency of Crick-Watson peak-peak distance was calculated and presented in **Figure 2b**. **Figure 2b** shows that the major cut sites on Crick and Watson within the same nucleosome tend to be paired, with distance equal to 2 and -5 nt respectively. (with the 5' to 3' direction defined as positive). If we regard that these cleavage peaks mainly arise from the primary and secondary sites, then there is only one possible configuration of the positions of the two sites that can give 2 and -5 nt distances. That is, for each DNA strand the free radicals must mainly cleave at sites -1 and +6 relative to the nucleosome center (position 0) (**Fig. 1c**). This configuration gives three different Crick-Watson peak-peak distances: 2 nt --- a cleavage peak at position -1 on both Watson and Crick; -5 nt --- a cleavage peak at position -1 on one strand and +6 on the other strand, and -12 nt --- a cleavage peak at position +6 on both Watson and Crick. The last distance (-12 nt) was not obvious in the peak-peak distance plot. This does not mean that the secondary site is not one of the major cleavage sites, but rather it tends to have lower average cleavages than the primary site (**Supplementary Fig. 1a**). As a result, there is only a small chance that the cleavages at the secondary sites from both strands are identified as the local maximum peaks simultaneously within the same nucleosome (as the peak-peak distance is defined). The -1 and +6 sites are referred to as primary and secondary sites respectively.

7. Single template weighted score

To identify the nucleosome centers based on the chemical data, we need to understand how the cleavages are distributed around primary and secondary sites within the nucleosome. Based on the primary-secondary sites configuration, we defined an eight-position weight template, measuring the relative cut frequency at four positions including (-2,-1,0,1) around the primary site (-1) and the other four positions including (4,5,6,7) around the secondary site (+6). These positions are denoted as $J = \{-2, -1, 0, 1, 4, 5, 6, 7\}$. Let $I = \{1, \dots, L\}$ be the set indexing genomic locations, and $W = \{W_i : i \in I\}, C = \{C_i : i \in I\}$ be the observed cut frequency on Watson and Crick respectively. We initialized the weights in the template model as

$$P = \{p_j : j \in J\} = (1/8, 1/4, 1/8, 0, 0, 1/8, 1/4, 1/8).$$

At each position $i \in I$, we calculated the template weighted score as

Eq. 1

$$s_i = \sum_{j \in J} (p_j W_{i+j} + p_j C_{i-j}).$$

We selected unique peaks of the template weighted score genome-wide as putative nucleosome centers using the same algorithm as described above in Section 6. Based on the selected nucleosomes, we updated the template weights P by the relative average cut frequency at the eight positions. These two steps were repeated until convergence. The converged template weights at the eight positions are (0.06, 0.26, 0.16, 0.056, 0.07, 0.14, 0.17, 0.08).

This approach is simple and effective in identifying well-positioned nucleosomes whose cleavage pattern shows clear primary-secondary configurations as shown **Supplementary Figure 4a**, in which scanning with this template will result in a characteristic score curve with three peaks. The middle highest peak corresponds to the center of a nucleosome. In contrast we observe clusters of many template score peaks in some regions (**Supplementary Fig. 4b**), suggesting there are multiple nucleosomes positioned in an overlapping manner. This approach becomes ineffective to identify the nucleosome centers in such clusters. In the following section, we shall use the identified well-positioned nucleosomes from this approach to train a single-template and develop a deconvolution approach to improve the nucleosome calls.

8. A convolution model and a Gibbs sampler approach for deconvolution

The presence of clustered cleavage frequency peaks on the same strand suggests that nucleosomes may exist in an overlapping manner. If the cut frequency from each nucleosome follows the template model as described above, then the observed cut frequency at a particular position is the summation of the cuts from closely clustered nucleosomes. Consequently, the template score defined above may not reflect the true likelihood of a nucleosome positioned at the given location.

To generalize our template weighted score approach, we hypothesized that every position can in principle be the nucleosome center (except the first or last 73 positions of each chromosome). We re-defined the average cut frequency of the eight positions of the template model in the absolute scale (it was defined in relative scale in the weighted score above) as follows:

$$\Lambda = \{\lambda^j : j \in J\},$$

where $J = (-2, -1, 0, 1, 4, 5, 6, 7)$. The average cut frequency in the trained template is presented in **Supplementary Figure 1a**.

A nucleosome positioned at i incurs cuts at Watson positions $i + j$, and at Crick positions $i - j$, for $j \in J$. We denoted the cuts as $X_i = \{X_i^j : j \in J\}$ and $Y_i = \{Y_i^{-j} : j \in J\}$ respectively.

Furthermore, we assumed that X_i^j and Y_i^{-j} follow a Poisson distribution with mean parameter $k_{i1}\lambda^j$ and $k_{i2}\lambda^j$ respectively, where k_{i1} and k_{i2} are defined as the Watson and Crick nucleosome center positioning (NCP) scores respectively at position i , measuring the nucleosome positioning signal strength relative to the average template. In theory these two scores should accord with each other since both measure the strength of nucleosome positioning signal at the same location. Nevertheless, we observed in some regions, the cut frequency on the Watson strand substantially differs from that on the Crick strand. Hence we

imposed a constraint on k_{i1} and k_{i2} such that $k_{i1} = k_{i2}\delta_i$, where $\delta_i = \sum_{j=i-73}^{i+73} W_j / \sum_{j=i-73}^{i+73} C_j$, is the ratio

of total number of cuts on the Watson and Crick strands in the region of $i \pm 73$. We denoted these parameters of interest as $K = \{k_{il} : i \in I\}$.

Due to the existence of clustered nucleosomes, X_i and Y_i are not observed, but instead, the cut frequency W_i and C_i on Watson and Crick as a summation of all $X_{i'}^j$ where $i' + j = i$, and all $Y_{i'}^{-j}$ where $i' - j = i$ for $j \in J$ respectively. The following is the convolution model:

$$\text{Eq. 2} \quad W_i = \sum_{j \in J} X_{i-j}^j + \varepsilon_{i1}, \quad C_i = \sum_{j \in J} Y_{i+j}^{-j} + \varepsilon_{i2},$$

where $\varepsilon_{i1}, \varepsilon_{i2}$ are the added noise term, also assumed to follow a Poisson distribution. Thus the distribution of W_i (or C_i) is a convolution of all individual distributions of X_{i-j}^j (or Y_{i+j}^{-j}) and the noise term. The noise term is defined to account for the background cleavages non-specific to the targeted nucleosome centers. More importantly we shall use it as a control to measure the nucleosome positioning signal strength to select nucleosomes. To simplify calculation in the following, we used the average of the lower half of the observed cut frequency in the region of $i \pm 73$ of each strand as the mean parameter of the Poisson noise, denoted as $\lambda_{i1}^0, \lambda_{i2}^0$ henceforth.

Assuming that all terms in the model are independent, then W_i and C_i have the following distributions:

$$W_i \sim \text{Poisson}\left(\sum_{j \in J} k_{(i-j)1} \lambda_{i1}^j + \lambda_{i1}^0\right), \\ C_i \sim \text{Poisson}\left(\sum_{j \in J} k_{(i+j)2} \lambda_{i2}^{-j} + \lambda_{i2}^0\right).$$

The likelihood is given by

$$\text{Eq. 3} \quad L(\mathbf{K}; W, C) = \prod_i f(W_i; \mathbf{K}) f(C_i; \mathbf{K}),$$

where f is the Poisson distribution mass function. Finding the maximum likelihood estimate of $\mathbf{K} = \{k_{il} : i \in I\}$ is difficult due to the complexity of the model. We proposed a Bayesian approach for deconvolution. We imposed an independent and identical exponential prior for each k_{il} as follows:

$$\text{Eq. 4} \quad \pi(k_{il}) = \frac{1}{\mu} \exp(-k_{il}/\mu), \mu = 0.2.$$

We set the hyper-parameter $\mu = 0.2$ (mean of the exponential distribution) because most of the genomic positions are not the center of nucleosomes, as manifested by much lower cleavage

frequency compared with the average cleavage frequency of the nucleosome template model. In practice we found the resulting nucleosome map is very resistant to the choice of hyper-parameter value because of the large magnitude of the cleavage frequency at positions around the primary and secondary sites of the nucleosomes.

The likelihood thus becomes:

$$\text{Eq. 5} \quad L(\mathbf{K}, \mathbf{W}, \mathbf{C}) = \prod_i f(W_i | \mathbf{K}) f(C_i | \mathbf{K}) \pi(k_{il}).$$

We used a Gibbs sampler approach to find the posterior mean of the \mathbf{K} . The conditional sampling formula is given by:

$$\text{Eq. 6} \quad \pi(k_{il} | \mathbf{W}, \mathbf{C}, \mathbf{K}_{-i}) \propto \pi(k_{il}) \prod_{j \in J} f(W_{i+j} | \mathbf{K}) f(C_{i-j} | \mathbf{K}).$$

At convergence, the posterior mean of $\mathbf{K} = \{k_{il} : i \in I\}$, denoted $\bar{\mathbf{K}} = \{\bar{k}_{il} : i \in I\}$, was calculated from 100 independent Monte-Carlo samples for each i .

Based on the NCP scores, we defined a unique map of nucleosomes using the method described in Section 9 below. We examined whether the cleavage pattern around the primary and secondary sites depends on the base composition in any nearby positions.

Interestingly we found four substantially different cleavage patterns determined by the base composition at -3 and +3 positions. More specifically, the four patterns can be labeled as A(-3)T(+3), -A(-3)T(+3), A(-3)-T(+3), and -A(-3)-T(+3), in which +/- in front of A/T stands for present/absent of nucleotide A/T at corresponding positions (**Supplementary Fig. 1b**). The cleavage pattern within each template is very consistent across different base compositions at each of the eight positions (**Supplementary Table 1**). The difference could be due to a bias arising from the chemical process. If so, then the resulting NCP score, $\bar{\mathbf{K}} = \{\bar{k}_{il} : i \in I\}$, will also be biased under the single template model. To account for this possible bias, we further trained four individual templates using the nucleosomes called from the deconvolution algorithm based on single template as described above. The average frequency at the eight positions of the four models is denoted as:

$$\Lambda_m = \{\lambda_m^j : j \in J\}, m = 1, 2, 3, 4,$$

where j is the eight positions defined above. At each genomic location, the applicable template model is pre-determined on each strand based on whether there is an “A” nucleotide at position -3 or a “T” at position +3.

We repeated the Gibbs deconvolution algorithm and computed the posterior mean of $\mathbf{K} = \{\bar{k}_{il} : i \in I\}$, denoted $\bar{\mathbf{K}} = \{\bar{k}_{il} : i \in I\}$ from 100 Monte-Carlo samples for each i . Under the four-template approach, the NCP score now reflects the positioning signal strength relative to the average cut frequency of each template.

9. Selection of unique and redundant nucleosome sets

We define the nucleosome center positioning (NCP) score at position i as the average of the Watson and Crick NCP scores, i.e., $\bar{k}_i = (\bar{k}_{i1} + \bar{k}_{i2})/2$. In addition, we define the average noise at position i as $\lambda_i^0 = (\lambda_{i1}^0 + \lambda_{i2}^0)/2$. We used the ratio of \bar{k}_i / λ_i^0 as the signal/noise ratio index for a positioned nucleosome at location i . At some positions, $\lambda_{i1}^0, \lambda_{i2}^0$ can be as small as near zero due to many positions in the $i \pm 73$ region having zero cleavage. Such tiny noise level could inflate a very small NCP score to a huge number, leading to unreasonable call of nucleosomes. Hence if the value of λ_i^0 is <0.5 , we set it as 0.5 to avoid over-inflation. We used a greedy algorithm to make nucleosome calls sequentially based on the magnitude of \bar{k}_i / λ_i^0 as follows. On each chromosome the position that had the largest \bar{k}_i / λ_i^0 was first called as the center of a nucleosome. Then another position with the largest \bar{k}_i / λ_i^0 among all positions that were at least ± 107 bp away from the first selected nucleosome was called as a nucleosome center. This step was repeated such that every selected nucleosome in the current step was at least ± 107 bp away from any previously selected nucleosomes. The algorithm stopped when no nucleosomes could be further called. By this approach, we allowed a maximum of 40 bp overlap between two neighboring nucleosomes. This could help reduce possible mis-calls due to mis-calls from previous rounds in the neighboring regions.

Based on the results from four-template model, we selected a total of 75,047 nucleosomes genome-wide, among which, 67,543 corresponding to 90% that have highest NCP score/noise ratio were further selected in the unique set to represent the collection of most likely nucleosome positions (**Supplementary Table 2**). In addition, we created a more

comprehensive redundant set by including all positions that have NCP score/noise ratio ≥ 0.40 , which corresponds to the smallest \bar{k}_i / λ_i^0 value from the unique map of 67,543 nucleosomes. In total 351,264 positions were selected (**Supplementary Table 3**).

The AA/TT/AT/TA signal from the unique map of four-template model is slightly but consistently better than that from the single-template model (**Supplementary Fig. 1c**), suggesting that the four-template model does provide better accuracy in the nucleosome map.

10. Nucleosome occupancy scores

The NCP score \bar{k}_i defined above provides a reasonable measure of the relative amount of nucleosomes centered at position i . Hence the nucleosome occupancy at position i , defined as the relative coverage by all possible nucleosomes, can be written as

$$\text{Eq. 7} \quad O_i = \sum_{j=i-73}^{i+73} \bar{k}_j.$$

The defined nucleosome occupancy is an evidence-based relative measure of the amount of nucleosomes coverage at each position. This is analogous to the reads occupancy commonly used in the MNase mapping, in which the nucleosome occupancy is measured by the number of reads that cover each genomic position. This occupancy is only meaningful in a relative sense when comparing different positions. Theoretically nucleosome occupancy should be defined as a probability that a given position on the genome is covered by any nucleosome¹⁴. It can be similarly calculated as in Eq. 7 by replacing \bar{k}_j with the absolute probability that the j th position is the center of a nucleosome. This probability is difficult to quantify because we lack a metric to normalize the NCP score into absolute probability measure. For example, consider two conditions where the nucleosomes are positioned at exactly the same locations. The occupancy at these positions however differs by a constant factor everywhere between the two conditions. Under the same sequencing effort (i.e. the total number of reads or cleavages) we expect to observe about the same number of cleavages at every nucleosome cleavage sites (subject to sampling variance) from the two conditions though the true occupancy probabilities are different everywhere between the two conditions. For this reason, we leave the NCP score as is without converting it into probability measure.

There are two issues in this definition. First, the occupancy can be affected by the bias arising from the gel extraction of the mapped genomic DNA fragments (as described in the **Main Text**). In some regions, particularly regions with long linkers (e.g. upstream of TSS), the cleavage cut frequency on one strand can be substantially lower than the other. As a result the NCP score on the strand with low cleave frequency tends to be under-estimated. We calculated the ratio of

$$\text{cleavage frequency of the two strands for every 147 bp region } (\delta_i = \sum_{j=i-73}^{i+73} W_j / \sum_{j=i-73}^{i+73} C_j \text{ defined}$$

above). Overall the cleavage frequency on the two strands is balanced, while in some regions there exists an uneven distribution (**Supplementary Fig. 3a**). To correct for this, we set the rule that if $|\log_{10}(\delta_i)|$ exceeds two standard deviations from 0, then the corrected NCP score is defined as $\bar{k}'_i = \max(\bar{k}_{i1}, \bar{k}_{i2})$, otherwise $\bar{k}'_i = (\bar{k}_{i1} + \bar{k}_{i2})/2$.

The second issue is the noise. In the raw data we observe low levels of chemical cleavages throughout the whole genome, many of which must correspond to non-specific or background cleavages due to DNA shearing during the experimental process or some other unknown reasons. In the deconvolution algorithm, we used the average of the lower half of cleavage frequency within every 147 bp window as an estimate of the noise level. This estimate could be conservative such that the resulting estimate of the NCP score may still carry part of the noise, which further aggregates to the occupancy score. This is less a problem in the nucleosome calls for the unique map, since they were defined based on the relative magnitude of NCP score/noise ratio (\bar{k}_i / λ_i^0). To control the noise in the occupancy, we set the same NCP score/noise ratio criterion as used in defining the redundant map (comprising ~350,000 nucleosomes, the set of nucleosome center positions is denoted as R below). Only the genomic positions in R will be regarded as having positioned nucleosomes with corresponding relative nucleosome amount of \bar{k}'_i . The bias corrected nucleosome occupancy score based on the redundant map thus is defined as

$$\text{Eq. 8} \quad O_i = \sum_{|j-i| \leq 73, j \in R} \bar{k}'_j.$$

The occupancy score in **Figure 4a** and **Supplementary Figures 8a** was defined using this equation. If we had not corrected for bias and controlled the NCP score/noise ratio, the occupancy curve would be noisier with higher baseline and have under-estimated occupancy

score at nucleosomes flanking long linkers (as suggested by **Supplementary Fig. 3b**, results not shown due to limit of space).

11. Additional details for different Figures

Figure 2

For the MNase 1 data¹, we first selected reads of length 137-157 bp to construct the center-weighted reads occupancy score. If a sequence length is odd, a Gaussian weight of $\exp[-0.5 * (d/20)^2]$ is assigned to a position d bp away from the center of the sequence for $d \leq 73$. If a sequence length is even, then the central two positions were treated as the center in turn to assign a weight $0.5\exp[-0.5*(d/20)^2]$ for a position d bp away from the center. We identified 26,155 well-defined peaks on the reads occupancy curve as putative nucleosome centers by controlling the peak height and steepness simultaneously.

For MNase 2², we followed the same approach except that we selected reads of length between 142-152 bp due to its much larger reads count. We identified 45,801 nucleosomes using a comparable criterion.

In **Figure 2c, 2d**, to compare different sets of called nucleosomes pairwise, we used one set as the reference to calculate the frequency of nucleosomes in the second set that are within d bp away from the closest nucleosome in the reference set for $-73 \leq d \leq 73$. The difference due to which set is used as the reference set is negligible.

Figure 3

In **Figure 3a**, we plotted the AA/TT/TA/AT signal of the nucleosomes that correspond to the four quartiles regarding the NCP score/noise ratio index (\bar{k}_i / λ_i^0).

In **Figure 3b**, the AA/TT/TA/AT signal for the MNase 1 was based on the alignment of selected nucleosome sequences of length 147 bp to achieve better signal.

Figure 4

Figure 4a: The TSS plot was based on the TSS collection¹⁵. Only the sites that were indicated with “complete” UTRs, in total 3017 were kept in this analysis. The MNase occupancy score was calculated using selected reads of length between 142-152 bp based on the uniform weight, i.e. the occupancy score at a given position is equal to the number of reads that cover this position. For the tRNA plot, only those tRNA genes without introns, 240 in total, were used to generate the plot.

Figure 4b: We defined the +1 nucleosome as the one that covers the ORF start site, and other classes accordingly. For the MNase curve, we first followed the same approach as in **Figure 2d** above to build center-weighted nucleosome occupancy curve for MNase 2 data. Using a less stringent threshold criterion than used in **Figure 2d**, we identified 64,198 peaks(to make the number of called nucleosomes comparable to chemical map) in the center-weighted occupancy curve genome-wide allowing at most 40 bp overlap between peaks by a greedy algorithm as in the unique chemical map. The selected peaks represent the approximate center positions of the nucleosomes, but often with systematic errors because of the well-known sequence preference of MNase. Hence if we had aligned the DNAs according to these peak positions, the AA/TT/TA/AT signal would become much weaker or even completely disappear. We instead searched for a sequence of length 147 bp nearest to the peak position in the +/-10 bp region. If no such sequence existed, we further searched for sequences of lengths 148, 146, 149, 145 and 150 bp sequentially within +/-10 bp region until the first sequence was identified. The center of the identified sequence was treated as nucleosome center to generate the AA/TT/TA/AT frequency plot. If no sequence was identified in +/-10 bp region, the peak position was treated as the true nucleosome center to generate the alignment.

Figure 5

Figure 5a: The top 50% nucleosomes were selected based on the magnitude of NCP score/noise ratio in the unique map of nucleosomes.

Figure 5b: For each nucleosome center i , we aligned the region from position $i - 250$ to $i + 250$ on the Watson strand with that on the Crick strand from position $i + 250$ to $i - 250$.

Figure 5c: We followed the Fourier transform approach¹⁶ to test the significance of 10 bp periodicity of the di-nucleotide signal in the flanking regions. We first calculated the Fourier

transform of the AA/TT/TA/AT signal in the core region based on 67,543 unique nucleosomes using $N = 2000$ (N is the length of time series). In the downstream flanking region of the alignment, we further calculated the Fourier transform for the alignment from position $147 + d$ to $147 + d + 179$ for fixed $d = 11, \dots, 20$ respectively. Likewise by assigning a random offset $d \in \{11, \dots, 20\}$ to each individual sequence we can obtain a random version of alignment of length 180 bp in the downstream region. The average and 95 percentile of the transform amplitude summarized based on 2000 random alignments are compared with the average transform amplitude from the alignments with fixed d .

Figure 6

Figure 6a: We used the map of regulatory factor sites¹⁷ (file p005_c1.gff, http://fraenkel.mit.edu/improved_map/latest_maps.html) to study the positioning of factor sites relative to the nucleosome centers. We first calculated the frequency of center-to-center distance, denoted $f(d)$, where $d = -73, \dots, 73$ if the factor length is odd, and $d = -72.5, \dots, 72.5$ if the factor length is even. The symmetrized frequency at distance d was defined as $f'(d) = f(d) + f(-d)$. We trained a position weight matrix for Abf1 factor motif, and used it to scan each nucleosome core sequence. The average score at each position is presented in **Figure 6a**.

Figure 6b: The binding site frequency plot for even length factors was generated by aggregating the symmetrized frequency of all even length factors. The center-to-center distance plot for Hermes transposon integration site was generated in the same way as the factor sites.

Figure 6c: We downloaded the two tracks of pre-processed RNAP pause data¹⁸ (in wig format), corresponding to the wildtype and $dst1-\Delta$ conditions. The pause scores were averaged at each nucleosome position from all nucleosomes in +2, +3, +4 classes.

Supplementary Figure 2

Supplementary Figure 2b: Given two sets of nucleosomes, we fixed one set, and calculated the fraction of the nucleosomes in the first set that were within $\pm d$ bp of any nucleosomes from the second set for $d \leq 70$. To compare with the random expectation, we further selected the

same number of random positions as in the second set for each chromosome. These random positions have to satisfy the constraints that they are representing legitimate centers of nucleosomes as in the original set. For example, for the chemical set, the distance between any two neighboring positions should be at least 107 bp away (allowing overlap up to 40 bp as in the chemical map), and for the MNase data, any two positions have to be at least 147 bp away.

Supplementary Figures 6 and 7:

The nucleosomes from the MNase 1 and 2 were defined as in Figure 3 above.

Supplementary Figure 9

See **Figure 4b** above.

12. Analyses based on redundant map using NCP score as a weighting factor

The chemical map not only provides a comprehensive set of preferential nucleosome positions genome-wide *in vivo*, but also their relative weights defined by the NCP scores. The NCP score can be regarded as a measure of the relative abundance of nucleosomes positioned at every genomic location in the entire cell population *in vivo*. Therefore we can use it as a weighting factor to investigate the nucleosome sequence features and its regulatory functions.

We confirm the results from **Figures 2e, 3a, 5a, 5b, 6a, 6b and 6c** based on the redundant map using NCP score as a weighting factor. The results are separately presented in **Supplementary Figure 12** (all other results can be similarly confirmed. They are not presented here due to space limits).

Supplementary Figure 12a

For the analysis of distance between clustered nucleosomes (**Fig. 2e**), we calculated the distance from every pair of nucleosomes in the redundant map (for distance ≤ 100 bp). Since the product of their NCP scores reflects the chance of the random combination of the two given nucleosomes in the cell population, we weighted the frequency of every resulting distance by the product of their NCP scores.

Supplementary Figures 12b,d

For nucleosome sequence feature analyses (**Figs 3a, 5b**), we center-aligned all nucleosomes from the redundant map. At each position of the aligned nucleosomes, the NCP score weighted average of AA/TT/AT/TA signal was calculated.

Supplementary Figure 12c

For the linker length analysis (**Fig. 5a**), we calculated the distance from every pair of nucleosomes in the redundant map (for distance >147 bp). Same as in **Supplementary Figure 12a**, we weighted each distance by the product of their NCP scores in the calculation of linker length distribution (linker length = nucleosome-nucleosome distance -147).

Supplementary Figures 12e,f,g,

For distance between nucleosome and any other site including regulatory factor binding, Hermes transposase binding, and RNAP pausing (**Figs 6a, 6b and 6c**), each observed distance was weighted by the NCP score of the given nucleosome.

Supplementary References

1. Field et al. Distinct modes of regulation by chromatin encoded through nucleosome positioning signals. PLoS Comput Biol (2008) vol. 4 (11) pp. e1000216
2. Floer et al. A RSC/nucleosome complex determines chromatin architecture and facilitates activator binding. Cell (2010) vol. 141 (3) pp. 407-18
3. Yager et al. Salt-induced release of DNA from nucleosome core particle. Biochemistry (1989) vol. 28 pp. 2271-2281
4. Widom. Role of DNA sequence in nucleosome stability and dynamics. Q Rev Biophys (2001) vol. 34 (3) pp. 269-324

5. Thåström et al. Nucleosomal locations of dominant DNA sequence motifs for histone–DNA interactions and nucleosome positioning. *J. Mol. Biol* (2004) vol. 338 pp. 695-709
6. Teif and Rippe. Predicting nucleosomes positions on the DNA: combining intrinsic sequence preferences and remodeler activities. Predicting nucleosome positions on the DNA. *Nucleic Acid Research* (2009) vol. 37 (17) pp. 5642-5655
7. Sidorva et al. Trapping DNA-protein binding reactions with neutral osmolytes for the analysis by gel mobility shift and self-cleavage assays. *Nucleic Acid Research* (2005) vol. 33 (16) pp. 5145 – 5155
8. Ou et al. Effects of osmolytes as folding aids on creatine kinase refolding pathway. *The International Journal of Biochemistry and Cell Biology* (2002) vol. 34 pp. 136-147
9. Escara and Hutton. Thermal stability and renaturation of DNA in dimethyl sulfoxide solutions: Acceleration of the renaturation rate. *Biopolymers* (1980) vol. 19 (7) pp. 1315-1327
10. Zhang et al. A packaging mechanism for nucleosome organization reconstituted across a eukaryotic genome. *Science* (2011) vol. 332 pp. 977-980
11. Flaus et al. Mapping nucleosome position at single base-pair resolution by using site-directed hydroxyl radicals. *Proc Natl Acad Sci USA* (1996) vol. 93 (4) pp. 1370-5
12. Flaus and Richmond. Base-pair resolution mapping of nucleosome positions using site-directed hydroxy radicals. *Meth Enzymol* (1999) vol. 304 pp. 251-63
13. Boyle et al. High-resolution mapping and characterization of open chromatin across the genome. *Cell* (2008) vol. 132 (2) pp. 311-322
14. Segal and Widom. What controls nucleosome positions? *Trends Genet* (2009) vol. 25 (8) pp. 335-43

15. David et al. A high-resolution map of transcription in the yeast genome. Proc Natl Acad Sci USA (2006) vol. 103 (14) pp. 5320-5
16. Wang et al. Preferentially quantized linker DNA lengths in *Saccharomyces cerevisiae*. PLoS Comput Biol (2008) vol. 4 (9) pp. e1000175
17. MacIsaac et al. An improved map of conserved regulatory sites for *Saccharomyces cerevisiae*. BMC Bioinformatics (2006) vol. 7 pp. 113
18. Churchman and Weissman. Nascent transcript sequencing visualizes transcription at nucleotide resolution. Nature (2011) vol. 469 (7330) pp. 368-73

Supplementary Figure Legends

Supplementary Figure 1 | Chemical cleavage patterns and noise. **a**, A single-template model **b**, a four-template model trained to describe the chemical cleavage pattern around the nucleosome center. Each plot shows the average cleavage frequency from position -20 bp to 20 bp (5' to 3' direction) relative to the nucleosome center. The four-template model contains four separate templates specified by whether having an A at position -3, or a T at position 3 (a “-” in front of A or T stands for absence of that letter). It accounts for potential bias associated with base composition at -3/+3 positions in the chemical mapping technique (**see Main Text**). Each template was further simplified to contain only eight positions surrounding the primary and secondary sites, including -2, -1, 0, 1, 4, 5, 6, 7 in the Bayesian deconvolution algorithm. **c**, Plot of AA/TT/TA/AT dinucleotide frequency of 67,616 unique nucleosomes from the Bayesian deconvolution algorithm using the single-template model versus 67,543 unique nucleosomes using the four-template model. The latter shows slight but consistently higher amplitude of signal in the entire nucleosome region indicating improved mapping accuracy. **d**, Top: histogram of noise level, defined as the mean of the lower half of cleavage frequency in the +/-73 bp region of each strand at each given genomic location. Middle: plot of average noise level as a function of distance to the nucleosome center in the unique map. Bottom: histogram of NCP score/noise ratio, where the 0.40 is the smallest NCP score/noise ratio in the unique map and the cutoff line used to define nucleosomes in the redundant map. It should be noted that the NCP score was defined as a ratio parameter, measuring the cleavage frequency at each nucleosome relative to the average cleavage frequency defined in the templates. Thus the threshold value 0.40 actually corresponds to a value in the absolute scale roughly equal to 0.40 multiplied by the average frequency of the underlying template. If the noise level is <0.5, we set it as 0.5 in this calculation to avoid over-inflation of NCP score /noise ratio.

Supplementary Figure 2 | Pairwise comparisons between nucleosome maps. **a**, Distances between the nearest nucleosomes in pairwise comparisons of unique nucleosome maps. Shown are comparisons for: the combined chemical map with the MNase 2 map; and the two MNase maps (MNase1 and MNase 2) compared with each other. Nucleosomes from the MNase data were called based on the significant peaks in the reads occupancy curve. **b**, Alternative pairwise comparisons of chemical versus MNase or of two independent MNase nucleosome maps. Red: each comparison asks, given nucleosome locations in one map, what

fraction of nucleosomes in another map are located within k base pairs away, for $k = 0 \dots 70$ bp. Black: random expectation for that comparison.

Supplementary Figure 3 | Average cleavage frequency around TSSs on coding strand and non-coding strand in chemical mapping. **a**, Current 6 batches of chemical mapping data show an unbalanced cleavage pattern between the two strands at the two nucleosomes immediately flanking the long linker region (nucleosome free region) upstream of TSSs due to gel selection bias. **b**, A follow-up experiment with isolated and sequenced DNA fragments of larger molecular weight ($\sim 200\text{-}500$ bp) shows a balanced cleavage pattern between the two strands at the above two nucleosomes, confirming the cause of cleavage asymmetry in the current chemical data. However additional minor cleavage asymmetry was observed at nucleosomes farther away from the long linker region for the same reason. For example, the fragment that spans -2 and +1 nucleosomes on the coding stand or fragment that spans +2 and -1 nucleosomes on the non-coding strand tended to be selected against because their lengths likely exceeded 500 bp, causing lower average cleavage frequency on the coding strand at -2 nucleosome and on the non-coding strand at the +2 nucleosome. **c**, Total cleavages in log scale in every 147 bp tiled window from the follow-up data versus the current 6 batches of chemical data. Existence of multiple consecutive long linkers (>50 bp) could result in unmappability of nucleosomes between the long linkers in the current data. Such nucleosomes however are mappable in the follow-up experiment. This plot shows no obvious regions that have high cleavages in the follow-up data while having no or extremely low cleavages in the current data, suggesting the nucleosomes missed in the current map due to bias by gel selection are very limited.

Supplementary Figure 4 | Single template weighted score pattern for well-positioned nucleosomes and clustered nucleosomes. **a**, A well-positioned nucleosome results in a characteristic three-peak template weighted score pattern with the middle highest peak corresponding to the nucleosome center position. A single, well-positioned nucleosome also results in a dominant NCP score peak indicating the nucleosome center. **b**, Clustered nucleosomes produce many peaks in the template weighted score, causing difficulty in identification of true nucleosome centers. The deconvolution algorithm is able to identify three clear major NCP score peaks, defining three overlapping nucleosomes, separated by 10bp.

Supplementary Figure 5 | Dinucleotide sequence preferences of nucleosomes. **a**,

Frequencies of AC/AG/CA/GA/CT/GT/TC/TG (left) and CC/GG(CG/GC dinucleotides (right) by quartiles of NCP score/noise ratio in the unique nucleosome map (100% = highest NCP score/noise ratio). **b**, Frequencies of AA/AT/TT/TA dinucleotides for two sets of nucleosomes defined in this study: unique (black, 67,543 nucleosomes) and redundant map (red, 351,264 nucleosomes). **c**, Frequencies of AA/AT/TT/TA dinucleotides in redundant map compared to nucleosomes lacking both A(-3) and T(+3) selected from redundant map. The latter were selected based on the NCP score/noise ratio requiring two neighboring nucleosomes to have no more than 40 bp overlap as in the unique map.

Supplementary Figure 6 | Single nucleotide distributions in chemical and MNase

nucleosome maps. Frequencies of A and C nucleotides within nucleosomes, for the chemical, MNase 1 and MNase 2 maps. Nucleosomes are symmetric, thus the patterns for G and T nucleotides are the reverse of those for C and A, respectively.

Supplementary Figure 7 | Dinucleotide distributions in chemical and MNase nucleosome

maps. Frequencies of each of the 16 dinucleotides for the chemical map (red) and MNase 1 map (black).

Supplementary Figure 8 | Global features of the high-resolution nucleosome map. **a**,

Nucleosome occupancy in the chemical map relative to origins of replication, defined as centers of the ARS consensus sequence (left), relative to exon-intron (center) and intron-exon (right) junctions. **b**, NCP score at sites relative to the centromere starts (left, defined as start of CDE I), and centromere ends (right, defined as the end of CDE III). The sharp NCP score spikes indicate very localized nucleosome center positions relative to the centromere starts and ends. Both alignments are shown because of variable lengths of CDE II.

Supplementary Figure 9 | Frequencies of AA/AT/TT/TA dinucleotides for nucleosome classes -1, +1, +2 ...+8 from chemical map (red) compared with MNase 2 map (black).

Both maps show that nucleosomes in different classes possess comparable AA/AT/TT/TA signal. The chemical map, however, shows much stronger amplitude because of better mapping accuracy.

Supplementary Figure 10 | Higher order chromatin structure and nucleosome spacing.

Distribution of linker DNA length for nucleosomes that are only within coding regions.

Supplementary Figure 11| High-resolution nucleosome center positions relative to genomic features. **a**, Frequency of all odd length annotated transcription factor binding sites relative to nucleosome centers. **b**, Top: Fourier transforms of the frequency as a function of distance relative to nucleosome center for Hermes transposon integration sites and for RNA polymerase II pause sites for wildtype and *dst1*-Δ yeast strains, showing ~10 bp periodicities. Bottom: Hermes transposon average motif score by scanning the nucleosome DNAs with trained weight matrix highly correlates with the observed frequency of sites as a function of distance to nucleosome center, demonstrating a type of multiplexing of genomic information. **c**, Cross-correlation of RNAP pause sites between wildtype and *dst1*-Δ strains for all unique nucleosomes, showing peaks of cross-correlation at offsets of half DNA helical turns ($\pm 5, 15$, etc) bp. This means that RNAP pauses at opposite faces of the double helical DNA when backtracking is or is not allowed.

Supplementary Figure 12 | Confirmation of main results presented in Figures 2e, 3a, 5a, 5b, 6a, 6b and 6c of Main Text based on redundant map using NCP score as a weighting factor. **a**, NCP score-weighted center-to-center distance between nucleosomes, showing the same local clustering pattern of nucleosomes as shown in **Figure 2e**. **b**, Position-dependent frequencies of AA/AT/TA/TT dinucleotides weighted by the NCP score produced based on the redundant nucleosome map, plotted by quartiles of NCP score/noise ratio. The positive correlation of sequence signal and NCP score/noise ratio suggests stronger periodic dinucleotide signals are favored in more stable nucleosomes. **c**, Distribution of NCP score-weighted DNA linker lengths for all redundant nucleosomes (black) and for the top 50% redundant nucleosomes with highest NCP score/noise ratio (red). **d**, NCP score-weighted AA/AT/TA/TT dinucleotide frequencies in the nucleosome region and extended flanking regions based on the redundant map. **e**, Functional (occupied and evolutionarily conserved) TF binding sites occur with high probability at specific locations inside nucleosomes where sequence preferences match TF weight matrix. Left panel: NCP score-weighted center-to-center distance frequency between redundant nucleosomes and Abf1 factor binding sites. Right panel: NCP score-weighted average motif score by weight matrix for Abf1 within redundant nucleosomes. **f**, Left panel: NCP-score weighted frequency of all even length annotated functional TF binding sites relative to nucleosome centers. Right panel: NCP-score weighted frequency of Hermes

transposon integration sites relative to centers of nucleosomes in the redundant chemical map.

g, NCP-score weighted frequencies of RNA polymerase II pause sites inside redundant nucleosomes of classes +2 to +4 in the chemical map plotted relative to their distance from the nucleosome centers, for wildtype cells (top) and *dst1*- Δ cells (which lacks polymerase backtracking ability; bottom). Because of overlapping of nucleosomes in the redundant map, the classes are not well defined. Instead we defined classes +2 to +4 nucleosomes approximately as those whose centers were in the ORF region and within 74 bp to $74+167*2=408$ bp downstream of TSS (red – raw data, black – smoothed data)

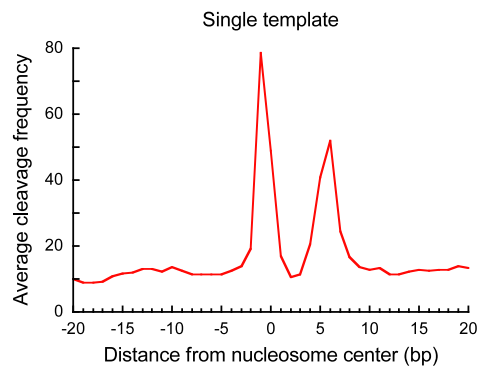
Supplementary Table 1| Average cleavage frequency across different nucleotides at each of the eight positions in each of the four templates summarized from the unique map.

Supplementary Table 2| List of nucleosomes in the unique map with NCP score and NCP score/noise ratio.

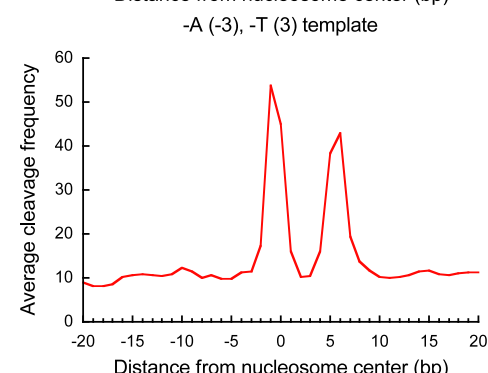
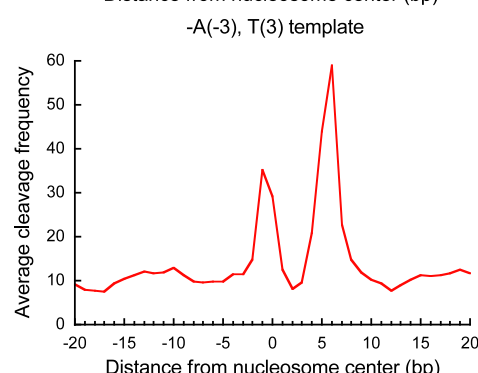
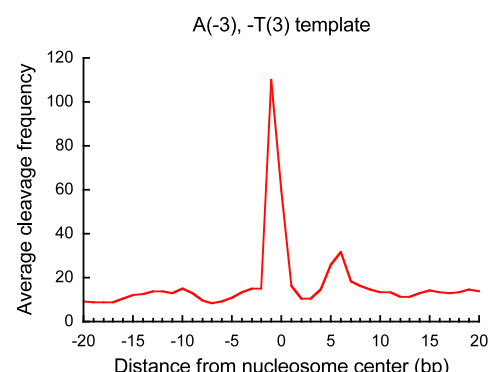
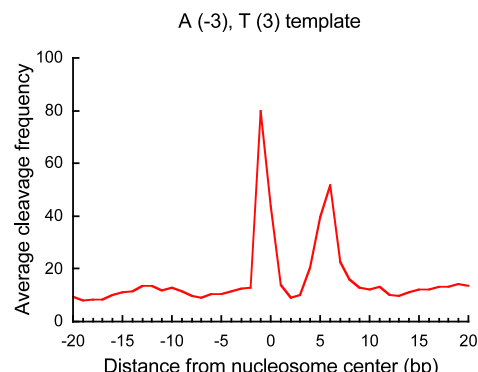
Supplementary Table 3| List of nucleosomes in the redundant map with NCP score and NCP score/noise ratio.

Supplementary Figure 1

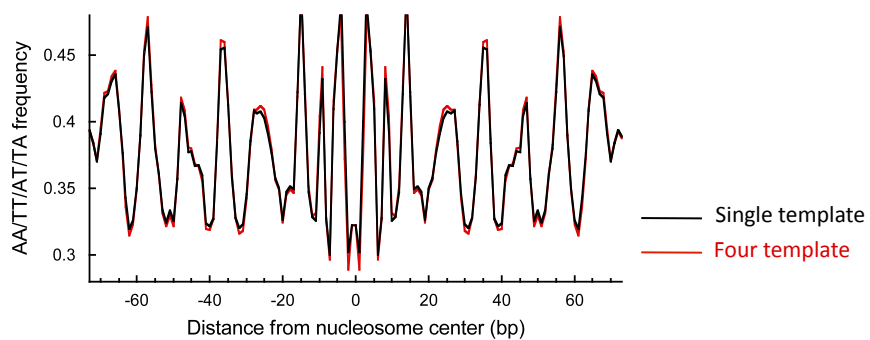
a



b

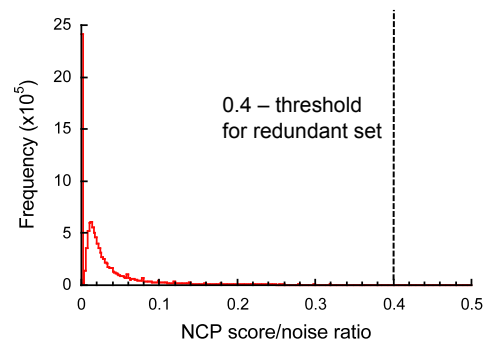
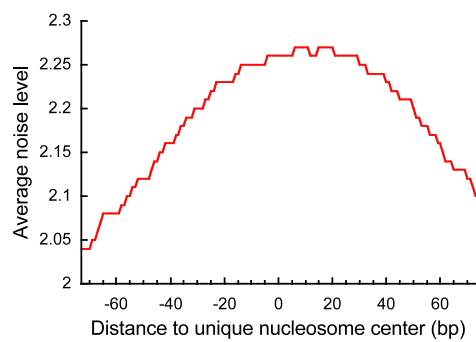
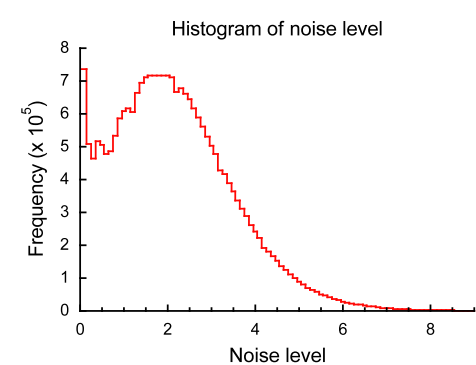


c

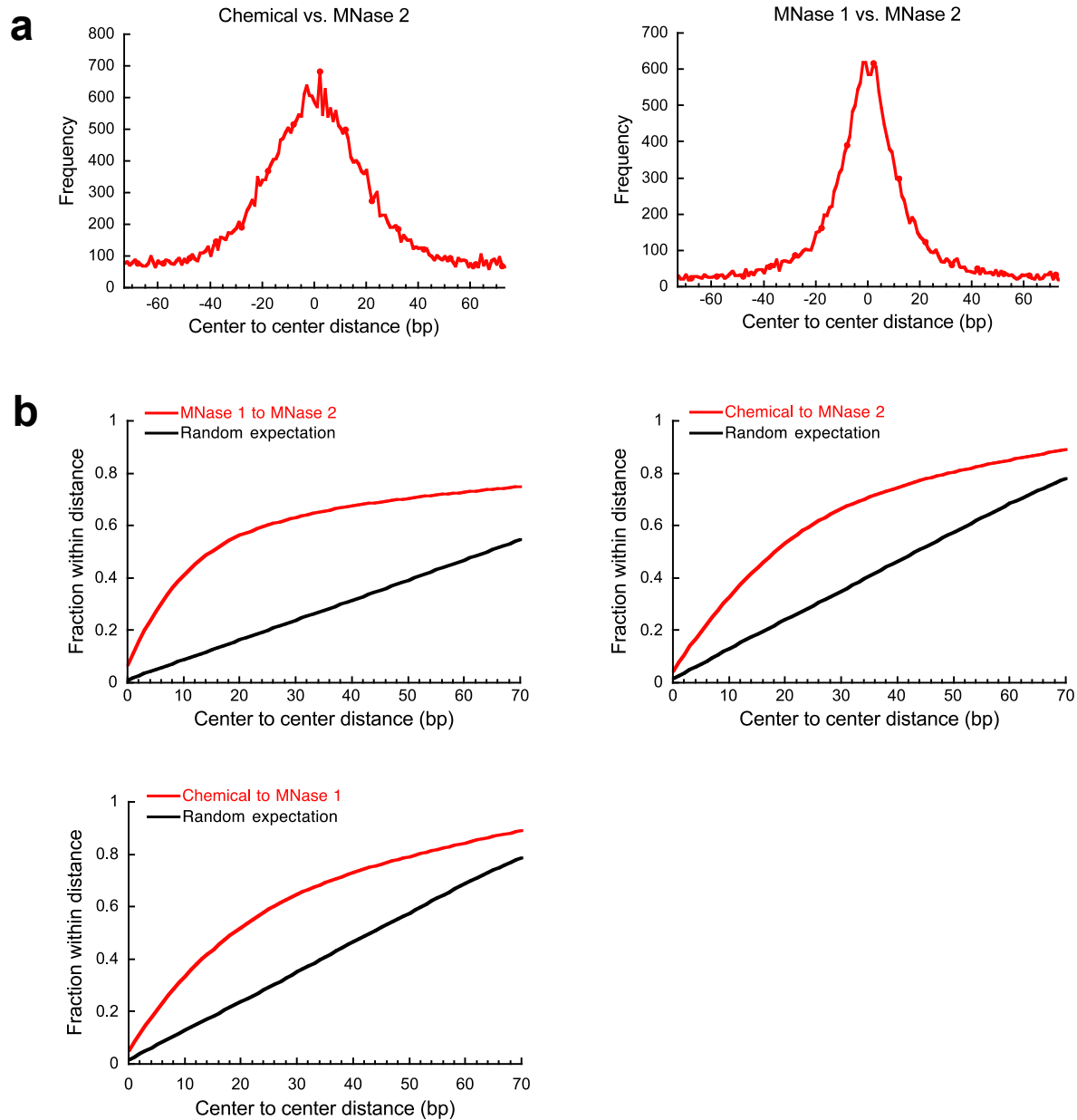


Supplementary Figure 1 continued

d

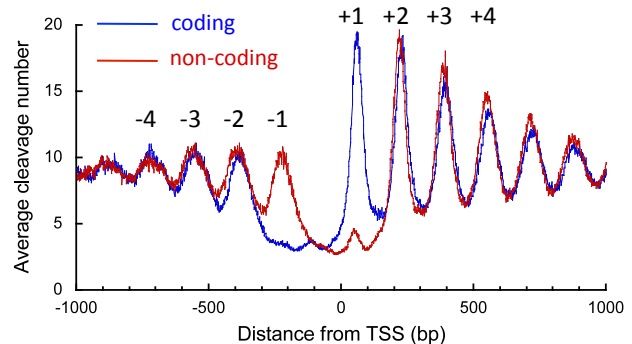


Supplementary Figure 2

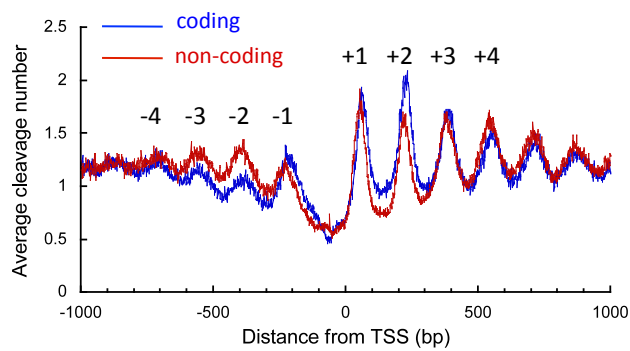


Supplementary Figure 3

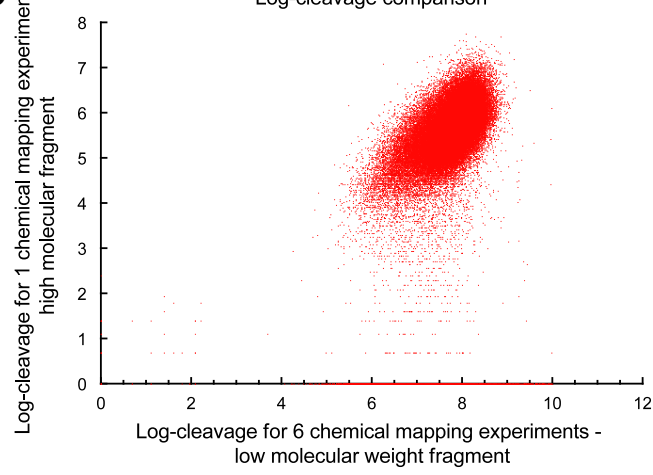
a Low molecular weight fragment - 6 independent chemical mapping experiments



b High molecular weight DNA - single chemical experiment



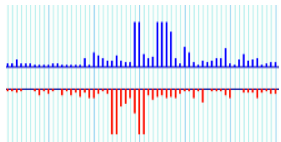
c Log-cleavage comparison



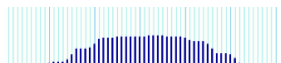
Supplementary Figure 4

a Single nucleosome

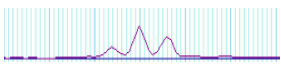
Chemical cut frequency Watson (blue)/Crick (red)



Chemical cut frequency +/- 15 bp moving average



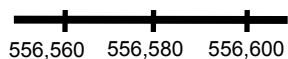
Template weighted score



Nucleosome center positioning (NCP) score

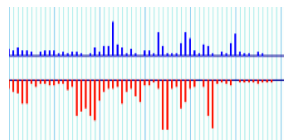


chrXVI



b Clustered nucleosomes

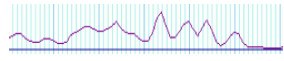
Chemical cut frequency Watson (blue)/Crick (red)



Chemical cut frequency +/- 15 bp moving average



Template weighted score



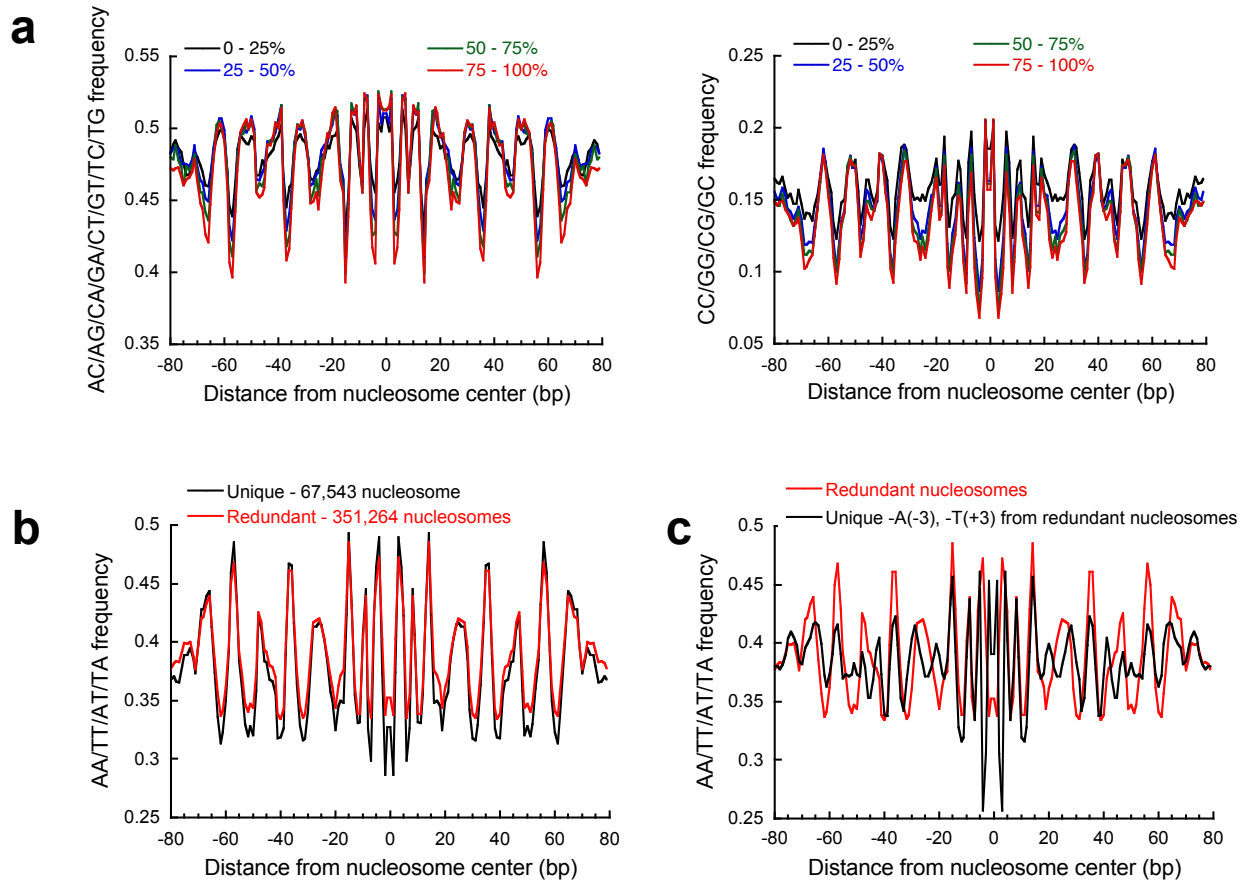
Nucleosome center positioning (NCP) score



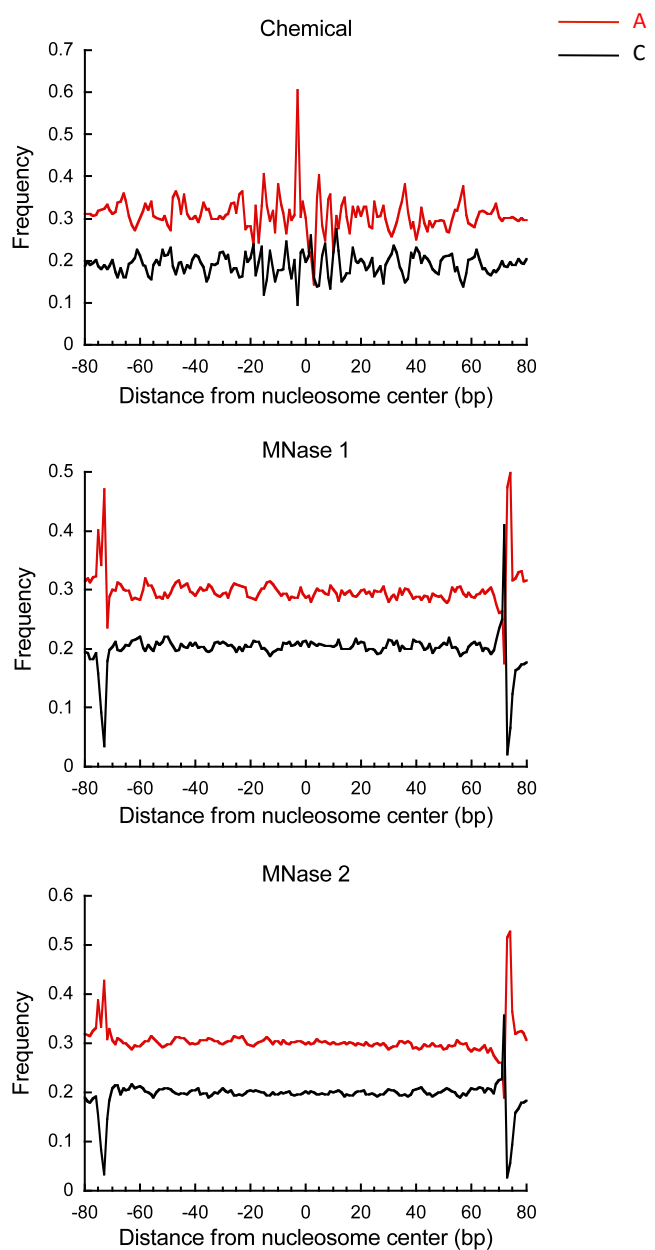
chrVII



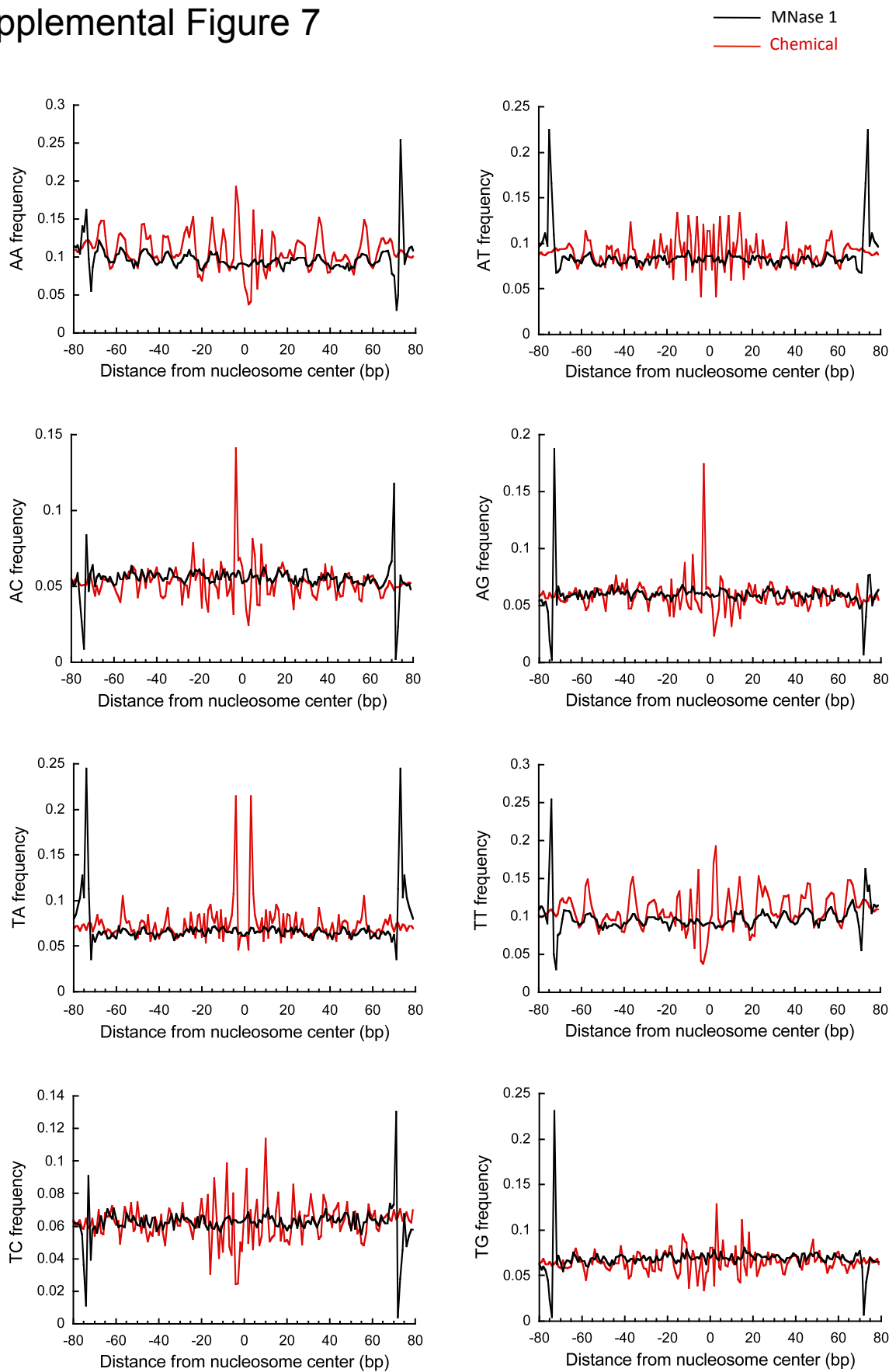
Supplementary Figure 5



Supplementary Figure 6

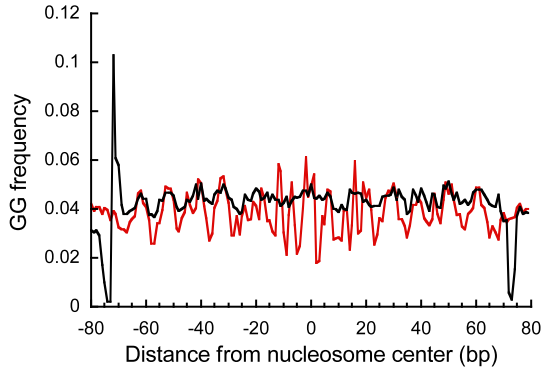
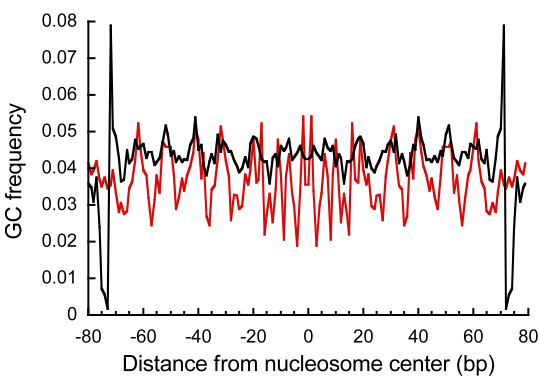
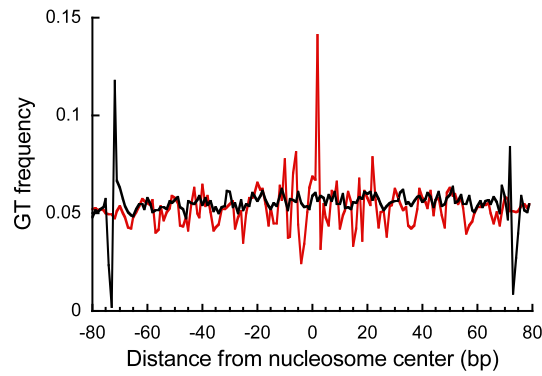
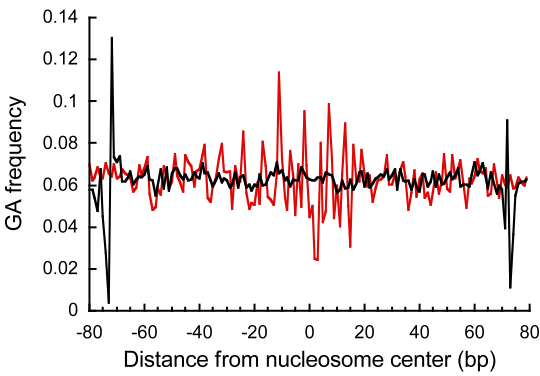
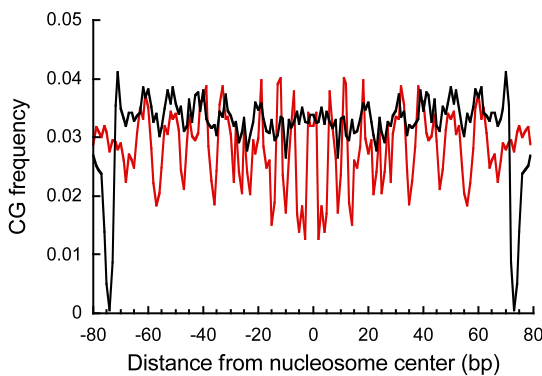
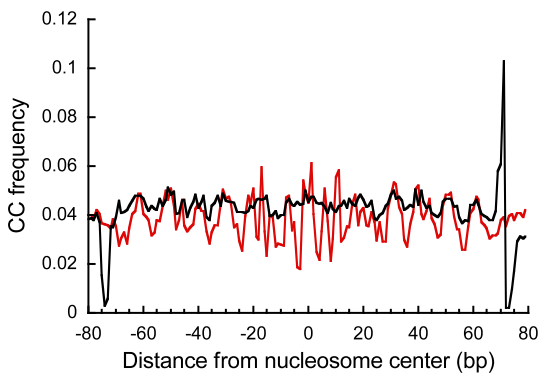
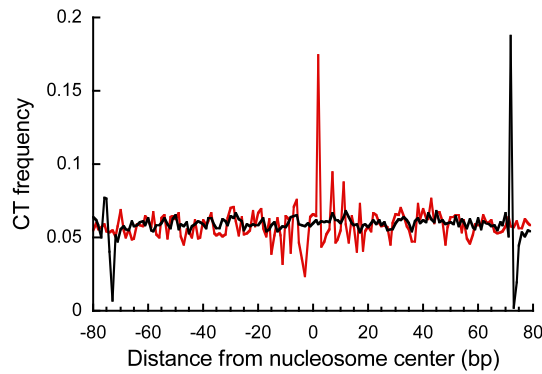
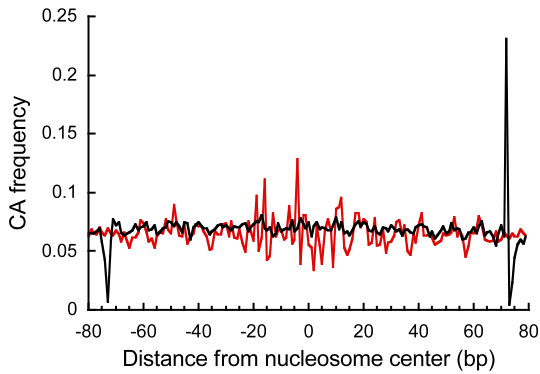


Supplemental Figure 7

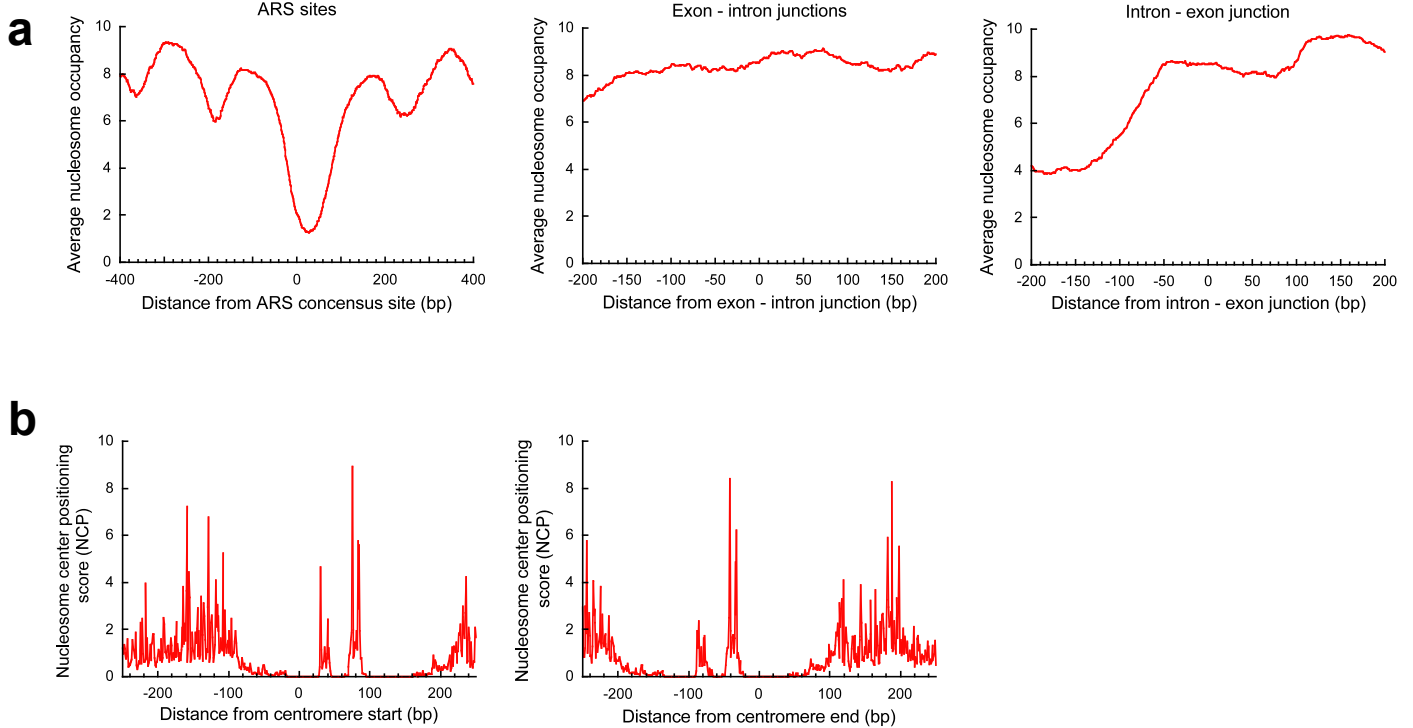


Supplemental Figure 7 cont.

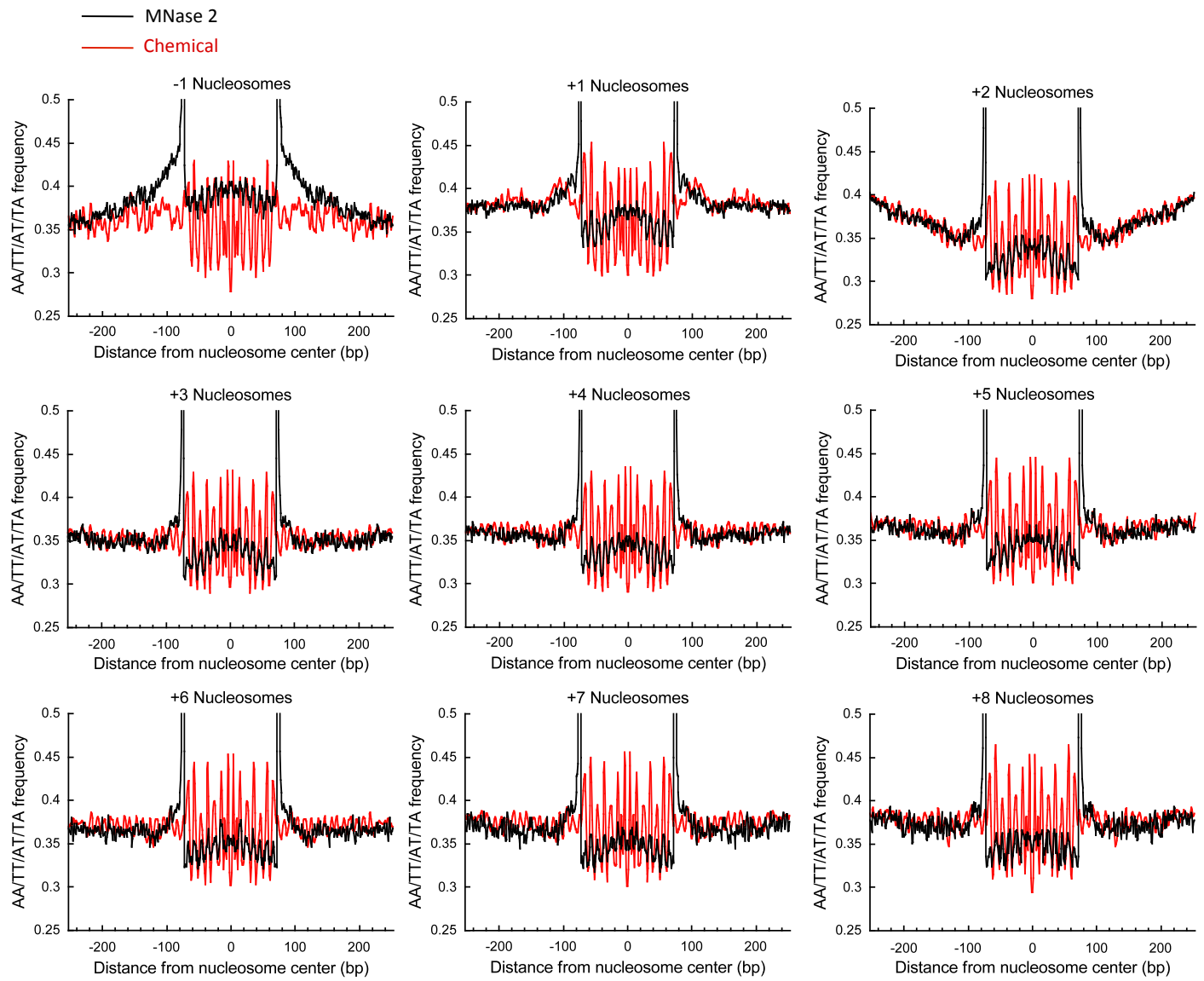
— MNase 1
— Chemical



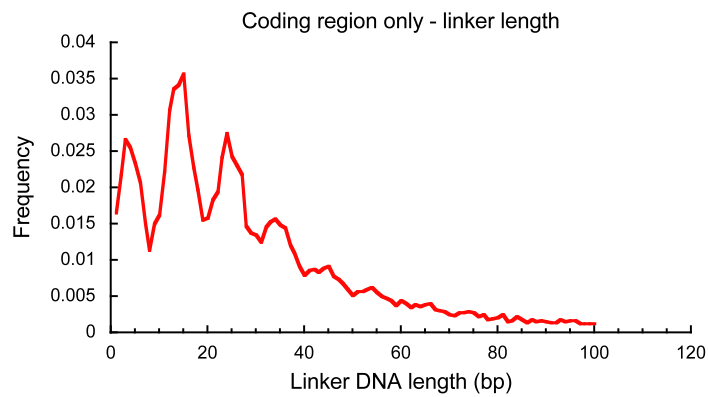
Supplementary Figure 8



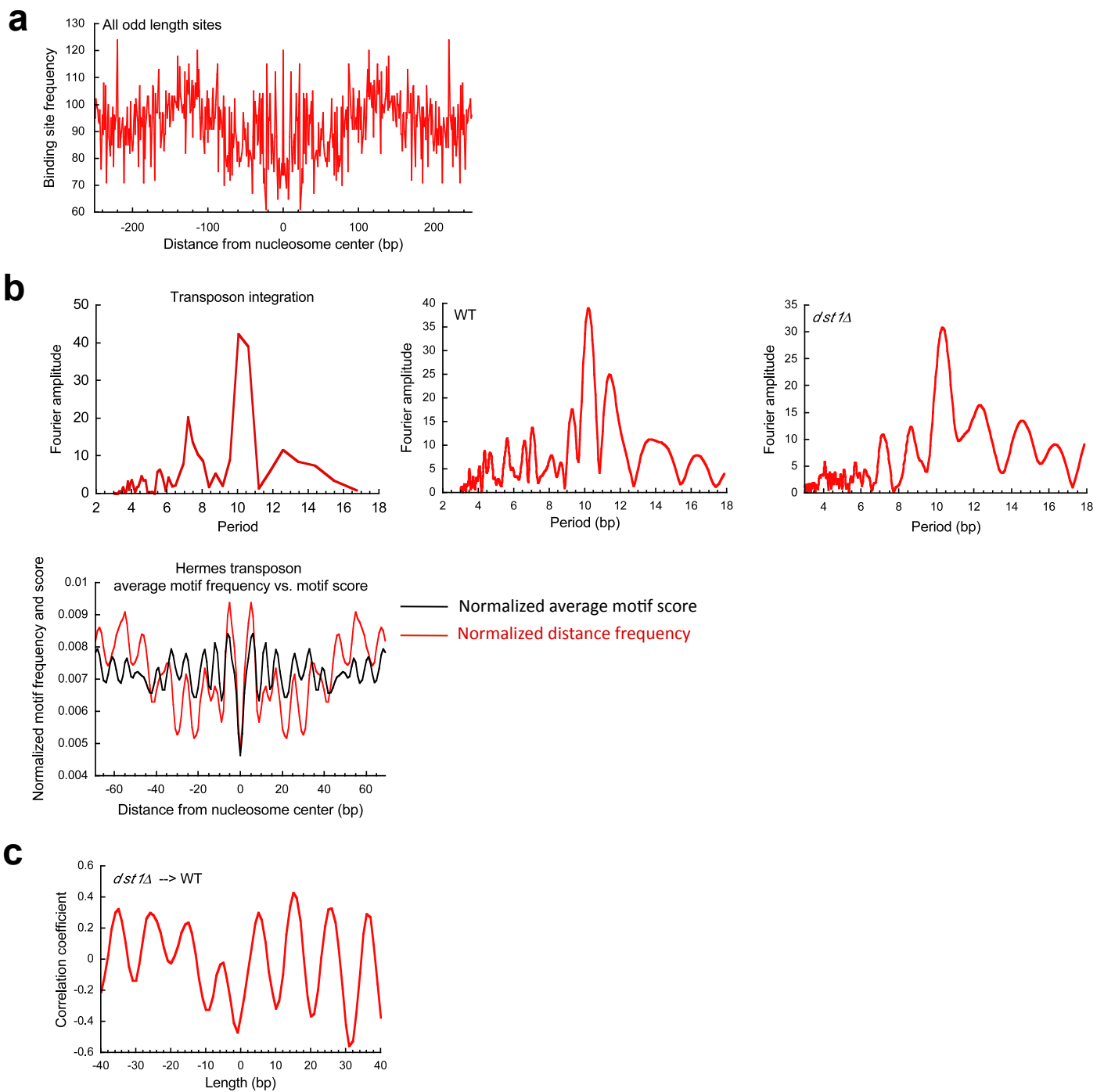
Supplementary Figure 9



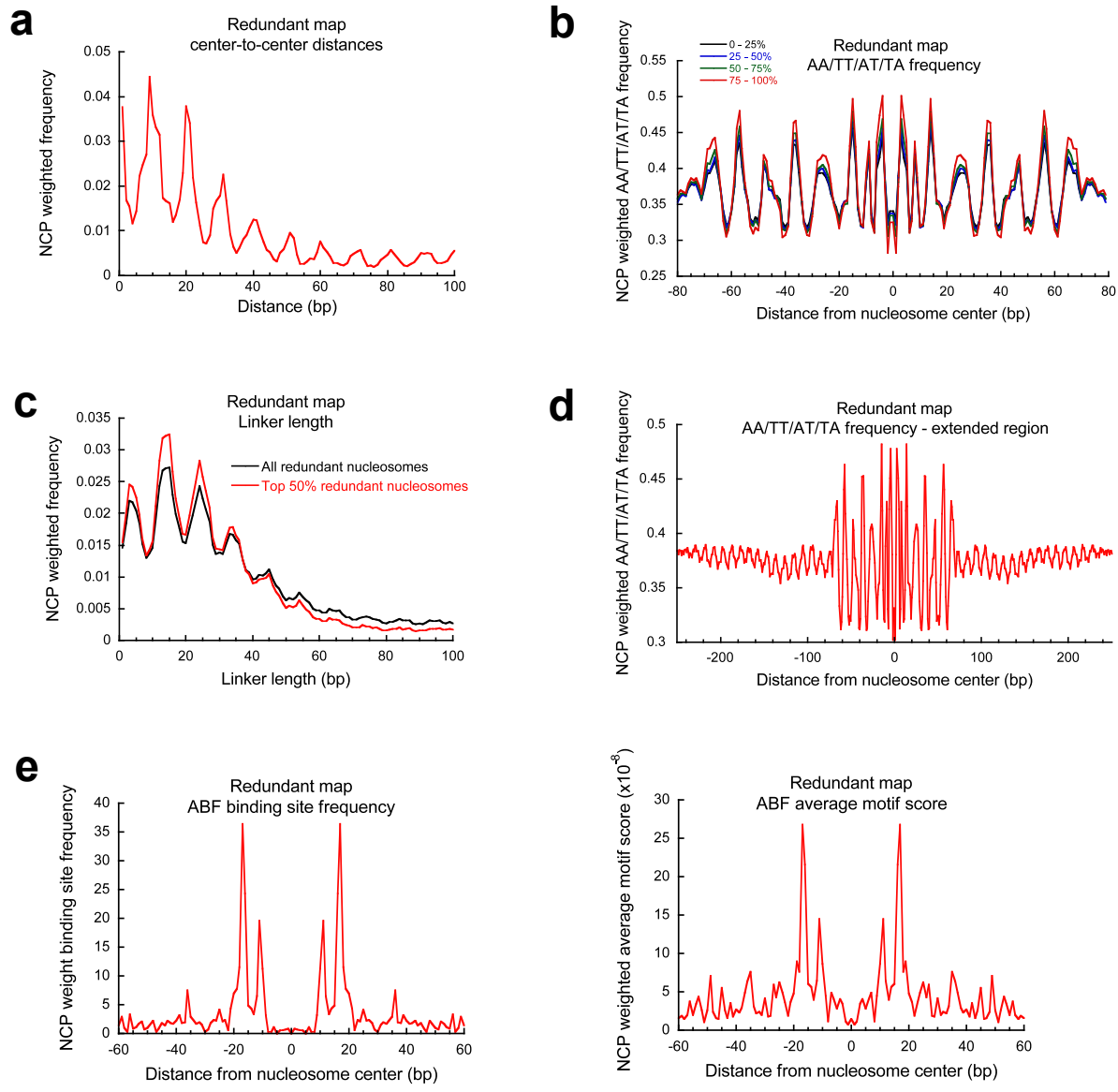
Supplementary Figure 10



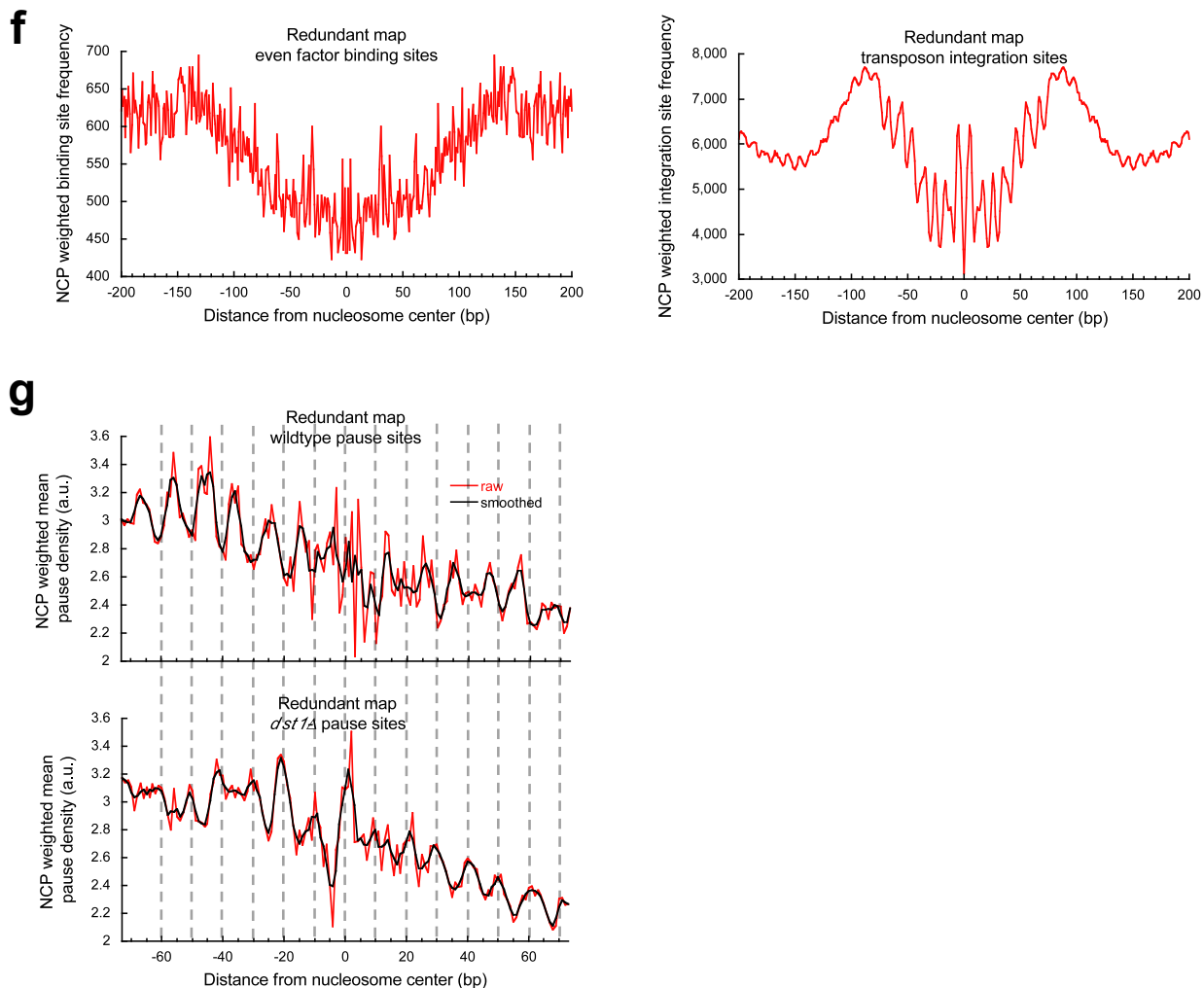
Supplementary Figure 11



Supplementary Figure 12



Supplementary Figure 12 continued



Supplementary Table 1| Average cleavage frequency across different nucleotides at each of the eight positions in each of the four templates summarized from the unique map.

A(-3)T(+3)	Position	A	C	G	T	Mean
	-2	13	13.7	11.3	14	13.0
	-1	82	84.3	77.6	72.9	79.2
	0	43.4	47	42	43.7	44.0
	1	14.8	15.3	13.9	12.6	14.2
	4	22.7	20.1	21.9	16.8	20.4
	5	44	34.8	34.8	39	38.2
	6	51.4	56	41.5	53.9	50.7
	7	22.6	24.5	20.6	22.4	22.5
A(-3)-T(+3)	-2	15.5	15.6	13.5	16.4	15.3
	-1	112.3	113.5	104.4	101.5	107.9
	0	60.8	62.3	52.2	60.9	59.1
	1	16.2	17.9	15.3	15.7	16.3
	4	16.1	13.3	12.7	14.9	14.3
	5	29.2	24.6	21.1	23.5	24.6
	6	31.7	33.4	26.1	33.2	31.1
	7	19.4	18.9	16.2	18.6	18.3
-A(-3)T(+3)	-2	15.1	15.5	15.4	14.1	15.0
	-1	36.1	36.7	33.1	33.8	34.9
	0	27.8	31.8	28.5	27.8	29.0
	1	13.3	13.8	12.6	11.2	12.7
	4	22.1	21	25	16.9	21.3
	5	48.2	38.4	39.9	43.1	42.4
	6	57.3	66.5	47.3	61.8	58.2
	7	22.7	26	20.8	22.6	23.0
-A(-3)-T(+3)	-2	19.4	18.9	19.5	18.7	19.1
	-1	56.2	58.7	53.7	55.1	55.9
	0	43.5	42.9	40.7	47.1	43.6
	1	15.5	16.7	13.8	15.5	15.4
	4	17.3	15.1	15.2	16.4	16.0
	5	41	44.6	36.4	32.7	38.7
	6	41.3	45.9	35.5	45.6	42.1
	7	19.2	19.3	17.3	17.9	18.4